

ISOMERIZATION OF LIMONENE ON ZEOLITE-CONTAINING CATALYSTS BASED ON KAOLIN

Lyubov Patrylak^{1,2,3*}, Stepan Zubenko¹, Serhy Konovalov¹, Anzhela Yakovenko¹,
Volodymyr Povazhnyi¹, Oleksandra Pertko¹, Yulia Voloshyna¹,
Oleksandr Melnychuk¹, Mykhailo Filonenko^{1,3}

¹V.P. Kukhar Institute of Bioorganic Chemistry and Petrochemistry of National Academy of Sciences of Ukraine,
1, Murmanska str., Kyiv 02094, Ukraine

²National Technical University of Ukraine "Igor Sikorskyi Kyiv Polytechnic Institute",
37, Peremohy ave., Kyiv 03056, Ukraine

³National Pedagogical Dragomanov University, 9, Pyrogova str., Kyiv 01601, Ukraine
*e-mail: lkpg@ukr.net

Abstract. The aim of the work was to study the isomerization of limonene on zeolite-containing biporous acid catalysts based on kaolin. Zeolite catalysts were synthesized from Ukrainian kaolin and characterized by using XRD, XRF, DTA/TG, IR-spectroscopy, low-temperature nitrogen adsorption, and pyridine sorption. Micro-mesoporous materials isomerize limonene at 160°C. The main reaction product on acid catalysts was terpinolene, while the original metakaolin microsphere catalyzes mainly the limonene condensation. The maximum yield of isomers is of 60–65% at 80–90% conversion. The obtained results show that the studied samples do not have a significant accumulation of carbonaceous deposits because limonene has high solubility, which helps to remove intermediate products of transformation from the surface of the samples.

Keywords: kaolin, zeolite, limonene isomerization, terpinolene yield.

Received: 20 June 2022/ Revised final: 08 September 2022/ Accepted: 14 September 2022

Introduction

Terpenes and terpenoids are well-known substances of biological origin, which until now have been used mainly as additives to perfumes with antiseptic properties. However, in recent years, a new trend has emerged regarding their possible use in bioprocessing to produce valuable chemicals [1,2]. Thus, the well-known "green" solvent limonene, obtained as a by-product of citrus processing and the paper industry, can be converted into *p*-cymene, a valuable intermediate for fine organic synthesis.

The conversion of limonene to *p*-cymene is still poorly understood. The modern idea about the mechanism of the transformation reaction of limonene into *p*-cymene consists of the sequential unfolding of isomerization of limonene into terpenoids (terpinolene, α - and γ -terpinene) and subsequent dehydroaromatization of the latter [3,4]. The process of isomerization of unsaturated compounds, in contrast to linear alkanes, requires catalysts with acid centers of not very high strength [5,6] or the use of lower process temperatures. Terpenoids are also valuable substances used in medicine and perfumery, as

well as in fine organic synthesis [7-12]. Terpinolene is an intermediate for the production of terpenoid acid [10-13]. It can be used to start and finish radical polymerization reactions involving unsaturated monomers [13].

Limonene transformation has been investigated using natural clay minerals [14-16] and titanium-containing mesoporous molecular sieves [17,18]. Approaches to the activation of the limonene molecule on Brønsted acid centers associated with titanium were proposed [17]. Quantitative conversions were achieved at the transitions from 150–160°C and 170°C, but only for 23–24 hours of the process. In all cases, considerable polymerization is observed on the source clays, and the yields of isomerization products are low (up to 20%), while additional modification with iron, manganese, and nickel ions significantly improves the selectivity for *p*-cymene. The synthesis of zeolites on the basis of kaolin allows for the combination of the zeolite phase and the matrix (residual kaolin) within the same sample, as well as the presence of micro- and meso-porosity [19].

The purpose of this study was to look into the isomerization of limonene using kaolin-based biporous acid catalysts containing zeolite, with improved diffusion properties.

Experimental

Materials

Kaolin (Prosyana deposit, Dnipropetrovsk region, Ukraine) was utilized for zeolite synthesis. The mineralogical composition of kaolin was as follows: 97 wt% of kaolinite, 3 wt% of mica, and quartz in trace amounts. The content of oxides in wt% was: 46% of SiO₂, 38% of Al₂O₃, 1.12% of Fe₂O₃, 1.16% of TiO₂, 0.12% of CaO, 0.28% of MgO, 0.6% of K₂O, 0.11% of Na₂O, 12.4% of H₂O.

The analytical grade reagents used in this study (NaOH, Ca(NO₃)₂·4H₂O, La(NO₃)₃·6H₂O, NH₄NO₃, Na₂SiO₃) were obtained from Ukrainian commercial sources and were used as received without further purification. Nitrogen and helium of high purity (99.99%) were applied in the measurements. In the experiments, pyridine and *n*-hexane (Sigma Aldrich, 99.0% for GC), as well as limonene (Merck, 98%), were used.

Methods and instruments

Synthesis of catalysts

In order to synthesize micro-mesoporous zeolites with improved diffusion properties, the latter were synthesized in situ in preformed kaolin microspheres (20–100 μm). To start with, the original kaolin was dispersed in water by adding sodium pyrophosphate. Ultrasound was used to improve homogenization. The formation of the microspheres (MS-1) from kaolin powder was performed using a disk spray dryer, in which the aqueous kaolin suspension was fed to the centrifugal disk and sprayed into the ascending stream of hot air (350–400°C).

By calcining microspherical kaolin at 730 and 1000°C for 2 hours metakaolin and a mixture of aluminosilicate spinel with reactive silicon oxide were obtained. The synthesis of zeolite of the faujasite type was carried out in the presence of an aqueous solution of alkali in accordance with the method described in [20]. Synthetic granules were prepared by mixing microspherical metakaolin with spinel and sodium silicate. The weight ratio of metakaolin to spinel was 1:1 or 1:2 for samples K1 and K2 respectively. Solutions of sodium hydroxide, seed (10% wt.), and additional water were added to granules. Amorphous seed (Na₂O/SiO₂= 1.0; SiO₂/Al₂O₃= 17.6; H₂O/Na₂O= 17.7) was pre-aged for 20 hours at 35–40°C. The syntheses were performed in glass flasks at 100°C for

20 hours. Then the granules were washed with hot water to pH= 9, dried at 100°C for 2 hours, and used as a basis for the preparation of the catalyst.

The catalysts were prepared by successive ion exchanges of the native zeolite sodium for calcium, lanthanum, and ammonium from aqueous solutions of nitrates of these salts (1, 1.5, and 3 mol/L) at 80–150°C for 3 hours. After each ion exchange, the samples were calcined in a muffle furnace at 550°C for 2 hours. Finally, the samples were further exchanged for ammonium without calcination.

The SiO₂/Al₂O₃ ratios according to X-ray fluorescence analysis were 2.1 and 1.6 for samples K1 and K2, which correspond to zeolite type X [21]. In terms of exchange capacity, the chemical composition of the synthesized samples was as follows (%): NH₄⁺(50), Ca²⁺(12), La³⁺(35), Na⁺(3) for K1 sample and NH₄⁺(40), Ca²⁺(17), La³⁺(40), Na⁺(3) for K2 sample.

Catalyst characterization

The porous properties of kaolin-based materials were assessed using low temperature (-196°C) nitrogen adsorption/desorption isotherms obtained with a Nova 1200e (Quantochrome) surface area and a pore size analyzer. Using nitrogen adsorption data at *p/p_s* values between 0.06 and 0.2, the specific surface areas (*S*^{BET}) were estimated using the conventional Brunauer–Emmett–Teller (BET) method [22]. The *t*-plot approach was used to determine the micropore volumes (*V*_{micro}^t) and micropore surface areas (*S*_{micro}^t). The Eq.(1) was used to get the average pore size *R*.

$$R = 2V^{\Sigma} / S^{BET} \quad (1)$$

where, *V*^Σ – the total pore volume, cm³/g;
S^{BET} – the specific surface area, m²/g.

The *R*^{BJH} is based on the Barrett–Joiner–Halenda (BJH) theory [23], while the *R*^{DFT} is based on the density-functional theory (DFT) [24].

The Lewis and Brønsted acidity of the samples was investigated using pyridine sorption with IR-spectroscopic control in the 1400–1700 cm⁻¹ range (Shimadzu IR Affinity-1S FTIR spectrometer). The samples were loaded into a special holder after being pressed into 5–10 mg tablets without a binder. The latter was then placed in a spectral cell, and the samples were activated for 1 hour in a vacuum at 380°C. The spectral probe was absorbed for 30 min at 150°C. To remove physically adsorbed pyridine, the latter was desorbed at 250°C for 30 min before recording IR spectra at 50°C.

The samples were subjected to *simultaneous thermogravimetric (TG) and differential thermal analysis (DTA)* in the temperature range of 20–1000°C using a Linseis STA 1400 system type derivatograph at a heating rate of 10°C/min. Calcined alumina at 1200°C was used as a reference material. Samples of 25 mg of zeolite were used in this study.

X-ray fluorescence analysis was used to determine the elemental composition of synthesized catalysts (Oxford Instruments X-Supreme 8000 analyzer, Great Britain).

The *diffraction pattern* of the original zeolite was recorded on a Rigaku MiniFlex600 diffractometer in CuK α radiation in the region of 2θ angles 2–80° with a step of 0.02° and a rotation speed of 5°/12 min. The acceleration voltage was 40 kV, and the anode current was 15 mA.

Catalytic testing

The limonene conversion was realized at atmospheric pressure in argon on a pre-activated catalyst in a closed system. The glass reactor tube was charged with 1.5 g of catalyst, and the unit was sealed. The catalyst was activated for 1.5 hour at 380°C in a vacuum. The reactor was heated using a sand bath with an electric stove. After cooling to 40°C, the argon supply was switched on until atmospheric pressure was reached and the magnetic stirrer was lowered into the catalyst bed (at the activation stage, the magnetic stirrer armature was held above the catalyst bed by a magnet). The glass stopper was opened and 10 g of limonene was loaded through the funnel, after which the hole was closed with a silicone stopper.

An oil bath filled with silicone oil was preheated on a heated magnetic stirrer to 160–170°C. After reaching the set temperature, the reactor was immersed in an oil bath and started stirring (speed 250 rpm). The reaction continued for 2–3 hours. Liquid samples were taken every hour.

Analysis of reaction products

Limonene conversion products were determined by using an Agilent 7890A gas chromatograph with a flame ionization detector, a split separator, and a J&W HP-5 capillary column (30 m, 0.32 mm, 0.25 μ m, (5% phenyl)–methylsiloxane). Liquid samples for analysis (about 0.05 g) were placed in a 4 mL vial and dissolved in 3 mL of *n*-hexane. Chromatographic analysis was performed under the following conditions: evaporator temperature – 250°C; flow separation – 30:1; carrier gas flow (helium) – 2.5 cm³/min (steady

flow mode); temperature program of the thermostat of the chromatographic column – 70°C/12 min – heating to 180°C at a speed of 120°C/min – heating to 320°C at a speed of 35°/min; detector temperature – 250°C; sample volume – 1 μ L. The concentration of the components in the catalyst composition was calculated as the ratio of the corresponding peak area to the sum of the areas of all the peaks represented in the chromatogram.

Results and discussion

Catalysts characterization

After all ion exchanges, zeolite-containing catalysts K1 and K2 have the same origin with only a slight difference in their chemical composition, which has been indicated above. According to silica to alumina ratio studies by X-ray fluorescence analysis, a zeolite phase is presented by low silica X-type zeolite. X-ray diffraction investigations have been conducted in order to confirm this. The XRD data for kaolin-based samples show the formation of crystalline phases (Figure 1). The main characteristic lines of the faujasite-type zeolites can be seen in the diffractograms of the samples synthesized from kaolin ($2\theta = 6.1, 9.9, 11.7, 15.4, 18.4, 20.0, 21.0, 22.5, 23.3, 23.5, 26.7, 29.1, 30.1, 31.0, 32.0, 33.5, 37.2^\circ$) [21]. Some X-ray amorphous halo is observed at the level of $2\theta = 25.0\text{--}30.0^\circ$ in kaolin samples, and may reflect the presence of unconverted metakaolin, which is X-ray amorphous. The peaks observed at $2\theta = 45.0^\circ$ and $2\theta = 67.0^\circ$ indicate the presence of aluminosilicate spinel in the samples. Thus, the XRD and XRF data show that the catalysts were synthesized from kaolin, with the zeolite phase represented by X-type zeolite with minor admixtures of aluminosilicate spinel. The SiO₂ to Al₂O₃ ratio is close to 2.

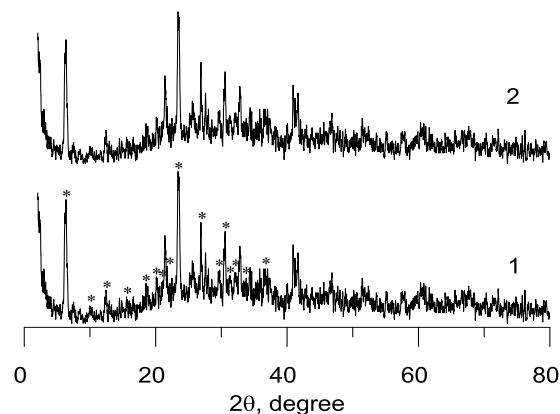


Figure 1. XRD patterns for K2 (1) and K1 (2) samples. (* - the main characteristic lines of faujasite phase).

Figure 2 depicts the low-temperature nitrogen adsorption/desorption isotherms for zeolite-containing catalysts and the original kaolin microsphere (MS-1).

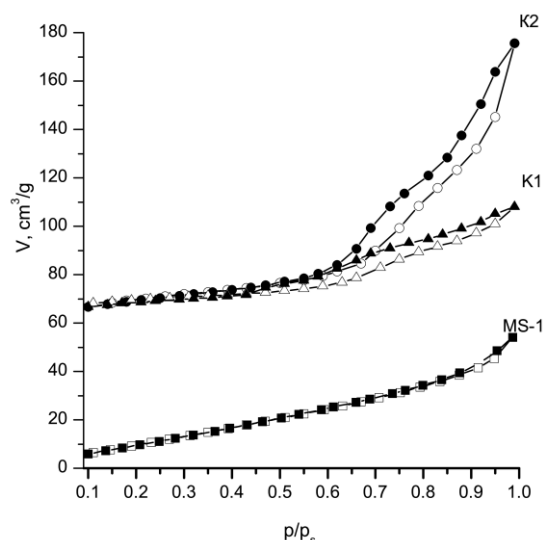


Figure 2. Isotherms of low-temperature nitrogen adsorption for a number of samples from kaolin.

According to the IUPAC classification, isotherms correspond to type IV and reflect the combination of microporosity and mesoporosity in the samples [22]. The latter is reflected by the presence of hysteresis loops of varying sizes caused by capillary condensation in mesopores ranging in size from 2 to 50 nm. Such a loop is

relatively weak in the case of the original kaolin microspheres (MS-1), larger in the case of K1, and the largest in the case of K2. The isotherm of the MS-1 sample clearly shows that there is no microporosity in the kaolin sample, as there is virtually no nitrogen adsorption at low saturation pressures. As a result, the synthesized catalysts are micro-mesoporous objects, also known as hierarchical zeolites.

From low-temperature nitrogen adsorption/desorption isotherms for kaolin-based zeolite-containing samples using BET, BJH, and DFT approaches, a range of the porous properties of the samples were calculated (Table 1). The specific surface area of kaolin microspheres MS-1 was initially 55 m²/g. Zeolite-containing samples based on it (K1, K2) have significantly higher specific surfaces of 250–260 m²/g.

The highest specific content of mesopores (74%) is in the sample K2 with the largest hysteresis loop. Distributions of pores by size, shown in Figures 3 and 4, demonstrate that the same sample has the largest dominant pores of about 3 nm according to BJH and 4 nm according to DFT.

Interestingly, for all samples synthesized in situ, the peaks of the predominant pores do not have sharp peaks and are quite wide, having many peaks of varying intensities, while in the case of synthetic zeolites, peaks are usually sharp, single, and much narrower.

Table 1

Adsorption characteristics of catalysts.									
	S^{BET} , m ² /g	S^t , m ² /g	S^{micro} , m ² /g	V^{micro} , cm ³ /g	V^2 , cm ³ /g	V^{micro}/V^2 , %	R^{DFT} , nm	$R^{BJH(des)}$, nm	R , nm
K1	252	34	217	0.10	0.17	62	1.1	1.8	1.3
K2	260	98	162	0.07	0.27	26	4.1	3.3	2.1
MS-1	55	33	22	0.02	0.08	22	2.4	1.5	3.1

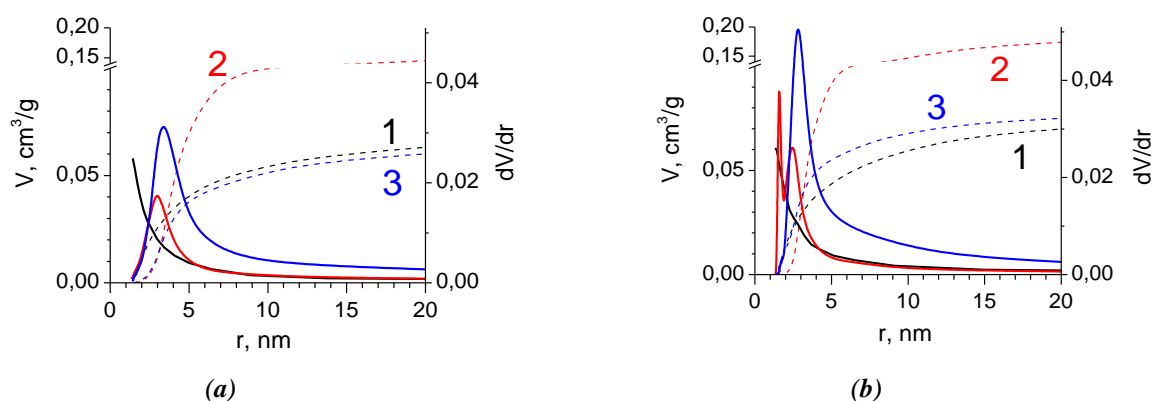


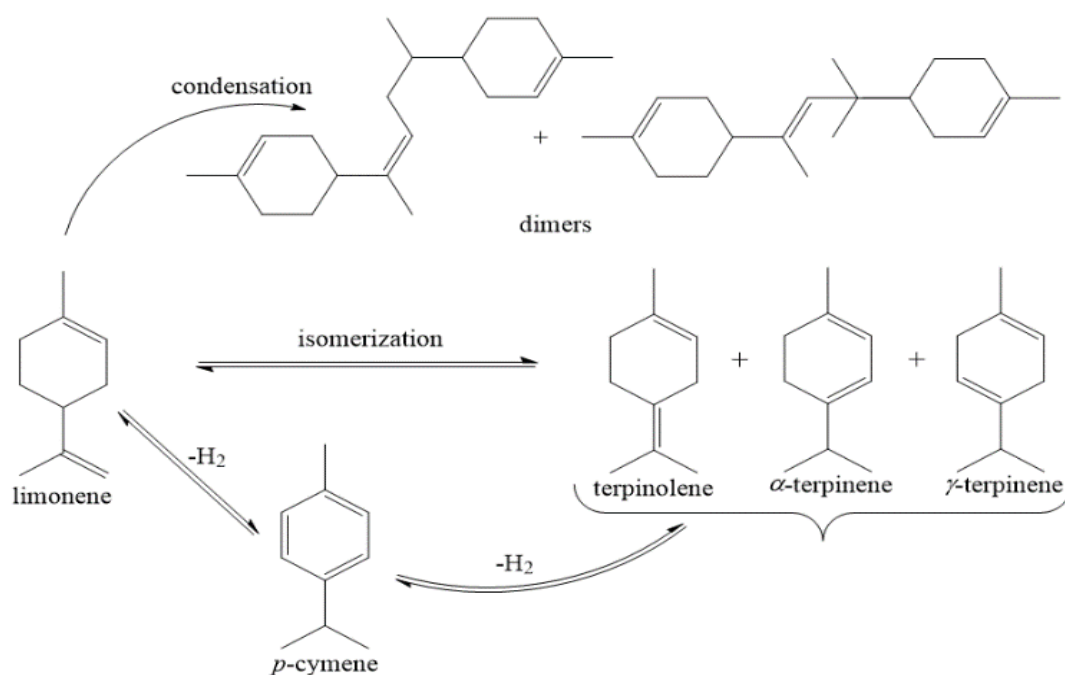
Figure 3. Integral and differential pore size distributions calculated from BJH theory using the adsorption (a) and desorption (b) branches of isotherms for MS-1 (1), K1 (2), and K2 (3).

Thus, the pore variance is larger for samples with an available binder or matrix component. Sample K2 has the largest volume of mesopores of 0.2 cm³/g, for other kaolin-containing samples, the range is from 0.06 to 0.08 cm³/g (Figures 3,4).

The total acidity of the samples was evaluated by following the sorption of pyridine under static conditions. The number of acid centers in mmol/g was 0.20, 0.90, and 1.04 for MS-1, K1, and K2, respectively. Figure 5 shows the acidity of the samples by sorption of pyridine monitored by IR spectroscopy. The bands at 1543 cm⁻¹ and 1454 cm⁻¹ indicate the presence of Brønsted and Lewis acid centers on the surface of the samples, respectively [25,26]. While the band at 1489 cm⁻¹ indicates both types of sites, Brønsted acidity dominates the catalysts. Based on the assumption that the Brønsted and Lewis acid centers represented by the band at 1489 cm⁻¹ are equally distributed, the number of Brønsted and Lewis acid sites was calculated to be 0.6 and 0.3 mmol/g for the K1 sample, as well as 0.68 and 0.36 mmol/g for the K2 sample. The total number of acid sites for samples K1 and K2 is comparable with the number of acid sites for powder faujasite-type zeolite (1.11 mmol/g) [5] or 1.2 mmol/g [27].

Isomerization of limonene

Limonene transformation can occur according to reaction Scheme 1 in a few ways. The original metakaolin microspheres MS-1 and the samples obtained on its basis showed different catalytic activities in the conversion of limonene (Figure 6).



Scheme 1. Possible ways of limonene transformation.

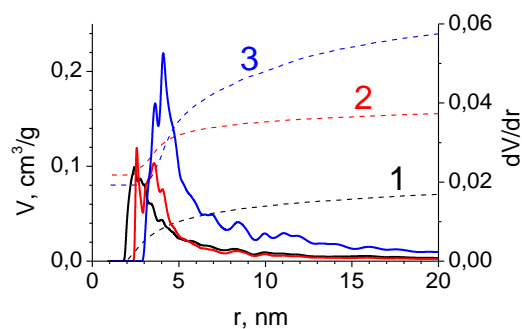


Figure 4. DFT-calculated integral and differential pore size distributions for samples MS-1 (1), K1 (2), and K2 (3).

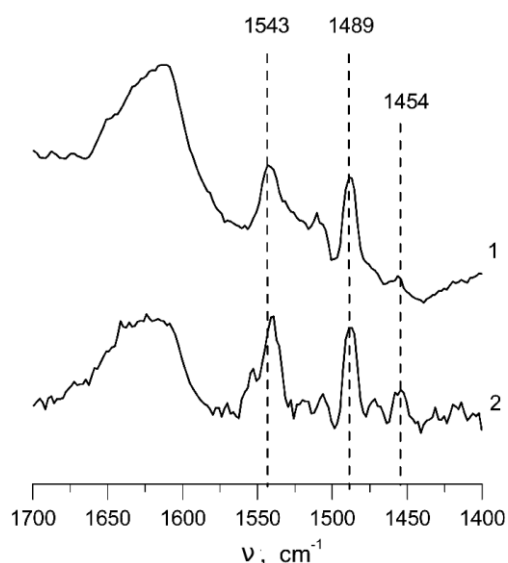


Figure 5. IR spectra of adsorbed pyridine on catalysts K1 (1) and K2 (2).

If the products on MS-1 for 50% conversion consisted primarily of terpinolene, with a selectivity of 50%, the process selectivity for this isomer dropped sharply to 10% for high conversions. In fact, the formation of dimeric compounds changes in antipath, increasing by up to 40%. Selectivity for α - and γ -terpinenes was 20% and 10%, respectively. There is an increase in selectivity for *p*-cymene up to 10% for the high limonene conversions. The latter from 90 min is more than 90%. As for the yields of the respective products, there is an opposite drop and an increase in the yields of terpinolene and dimers. The maximum yield of α - and γ -terpinene was observed for 90 min and was 18% and 15%. The yield of *p*-cymene increases linearly over time to 10% for 3 hours (Figure 6).

On the polycationic catalyst K2, the selectivity for terpinolene also decreases (Figure 7). However, the dimers are practically unchanged, and the selectivity for α -terpinene increases. The yields on this sample are higher and are up to 60% and 66% of isomers at 90 and 120 min.

Yields of dimers and *p*-cymene are low, up to 5% and 2%, respectively. Catalyst K1 shows lower conversions (up to 60% in 3 hours), increasing linearly over time (Figure 7(c)). The selectivity for all products changes only slightly with rising conversion. As a result, the yields of all products increase linearly (Figure 7(c)), the highest yields are being characteristic of terpinolene (up to 30%) and γ -terpinene (up to 15%). The total yield of isomers for 3 hours was 50%. This is higher than on the titanium-containing mesoporous molecular sieves (20%) at 150–160°C [17,18]. Values of selectivity for terpinolene on samples K1 and K2 are higher (up to 50%) than on the mesoporous zeolites (20–30% or 35–40%) [17,18]. Whereas α -terpinene selectivity is similar (20–30%).

Due to the fact that the K2 sample has greater mesoporosity, it achieves roughly the same performance at 90 min as the K1 catalyst does at 180 min. The peculiarities of the product distribution in favor of terpinolene observed on the samples indicate, first, that the isomerization of limonene to terpinolene is the simplest because the migration of the double bond occurs only within the alkyl radical in this case. This stage of the reaction is the first one according to the mechanism proposed in a previously published study [17]. The second reaction step is the transformation of terpinolene to α -terpinene and after that, the latter transforms to γ -terpinene. The obtained product ratios (terpinolene: α -terpinene: γ -terpinene: *p*-cymene) with a terpinolene predominance on the second hour (25:10:5:1) are similar to those reported in the literature (10:7:4:1) [17,18].

Further transfer of the double bond to the ring is much more difficult. Interestingly, also on MS-1, the yield of *p*-cymene increases in parallel with the increase in the yield of dimers. The latter may be due to the fact that similar to the alkylation reaction of isobutane with butenes, when the formation of a certain number of oligomeric compounds promotes hydride transfer, the saturation of hydrogen-unsaturated oligomers occurs due to the dehydrogenation of terpenes to form *p*-cymene. This process is less intense in the absence of a metal component, but it still manifests to some extent.

In the case of MS-1, terpinolene is first formed for up to 60 min, and then the process abruptly turns into dimerization. Apparently, the number of relatively strong Brønsted acid centers in metakaolin is so small that they are rapidly deactivated. After that, only centers, which can oligomerize the unsaturated compounds, remain on the surface of the sample.

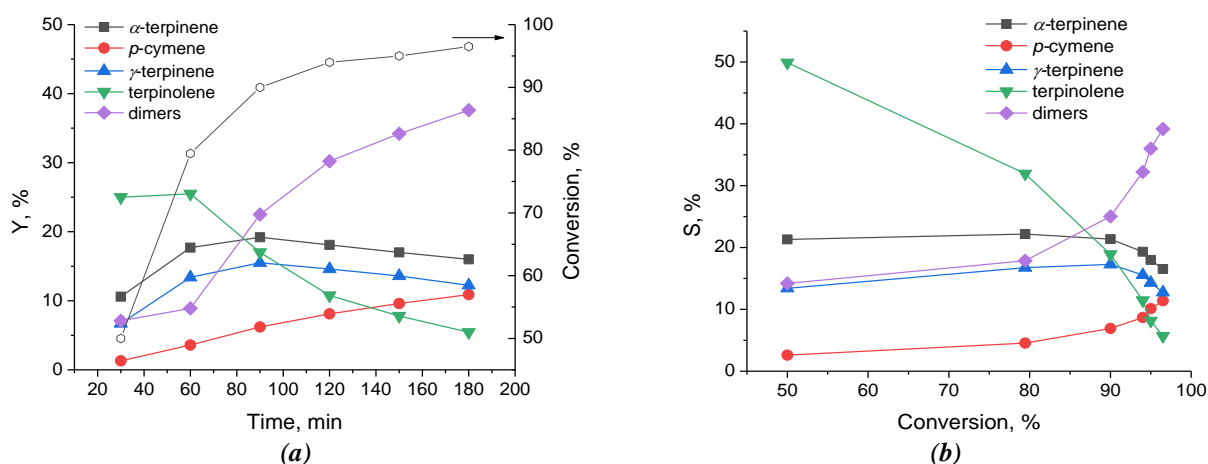
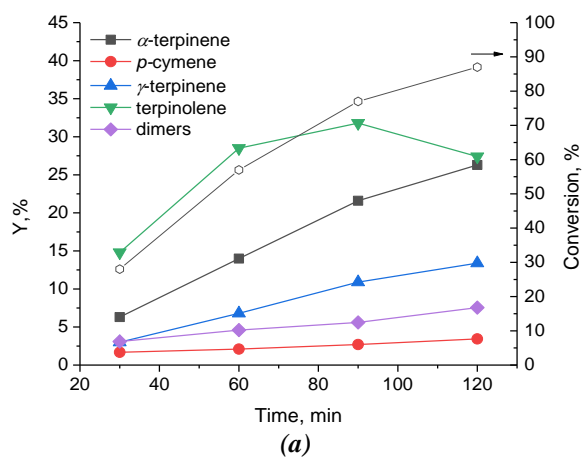


Figure 6. Conversion, product yields vs. reaction time (a), and selectivity vs. conversion (b) on the sample MS-1.

On acid zeolite catalysts, the acid centers are clearly stronger, and therefore the process is not aimed at dimerization, but isomerization of limonene. Furthermore, with a higher proportion of meso-porosity, the yields of isomers are higher in the case of the K2 catalyst (Figure 7).

As a result, limonene isomerization occurs properly not only on mesoporous molecular sieves [17,18], but also on catalysts that combine micro- and mesoporosity.



Investigation of deactivated catalysts

Figure 8 shows the DTA/TG curves for the samples studied in the conversion of limonene. After the reaction, the analyzed samples were washed with hexane. As can be seen from the DTA curves of samples K1 and K2 when heated to 400°C, endothermic minima are observed, indicating the process of desorption from catalysts at temperatures of approximately 100, 200, and 300°C.

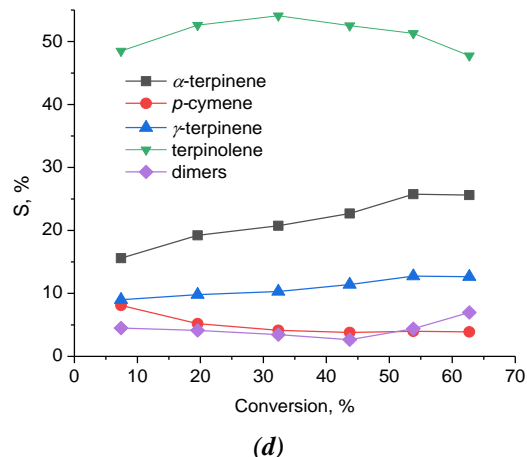
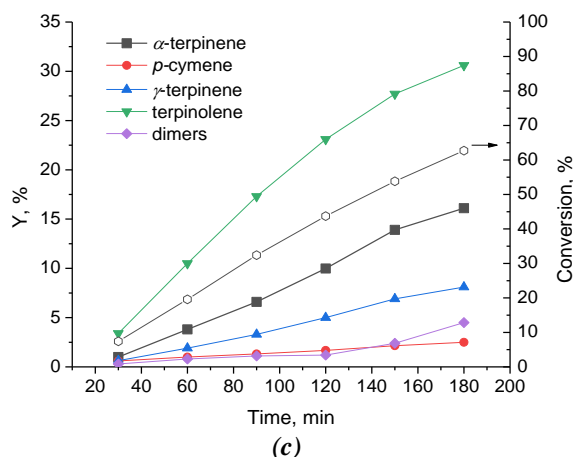
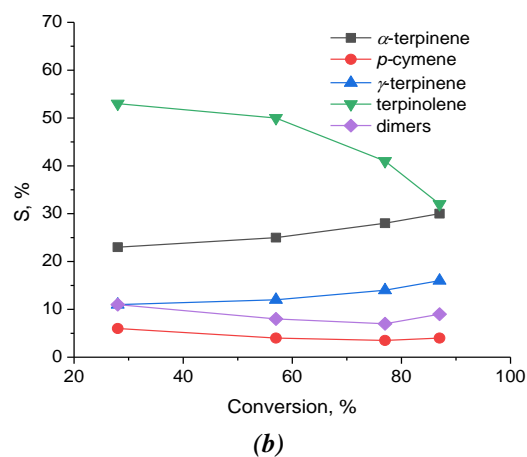


Figure 7. Conversion, product yields (a, c) vs. reaction time, and selectivity vs. conversion (b, d) on the samples K2 (a, b) and K1 (c, d).

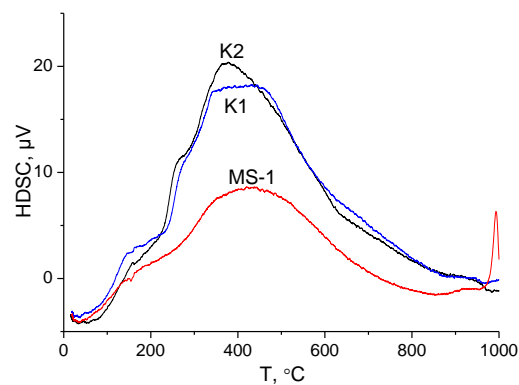
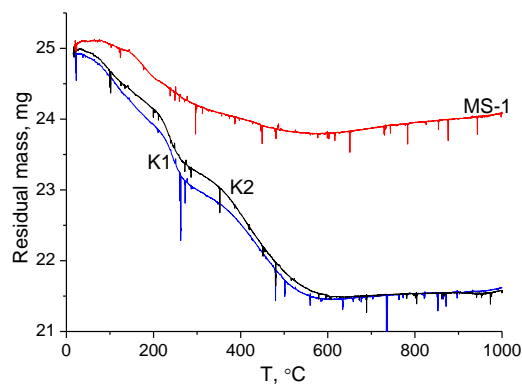


Figure 8. TG (a) and DTA (b) curves of MS-1, K1, and K2 deactivated samples.

There are three sections with different rates of weight loss: in the first and third, they are close, while in the second section, the speed increases. This appears to be due to the loss of various substances in the sample, at first glance. Hexane can be desorbed first, then limonene. However, the observed pattern is most likely caused by desorption from various structural elements, specifically the external surface of zeolite crystals, mesopores, and micropores. This assumption is confirmed by the existence of basically one desorption site in the case of the MS-1 microsphere sample, which has only mesopores. It is interesting that if for the first two samples, 3.5 mg were lost, which is 14%, in the case of MS-1, the weight loss was only 1 mg, or 4% of the mass. Whereas in the conversion of limonene, the largest number of dimer compounds were formed on it, which, however, were not retained on the catalyst, but were desorbed into the liquid medium. It is possible that this is due, firstly, to the low strength of the acid centers of MS-1, and secondly, to the high solubility of limonene as such. For both samples of the microsphere on the DTA curve, there is a

pronounced exothermic peak of about 950–980°C, which characterizes the phase transition [28].

In order to compare the changes that the samples underwent after the reaction was carried out, the catalysts were subjected to IR spectroscopy investigations. Figure 9 shows the IR spectra of fresh and deactivated samples in limonene isomerization. For all samples, the most intense absorption band is associated with antisymmetric valence vibrations of alumina-oxygen tetrahedra in zeolites and metakaolin [21]. Moreover, for zeolites, it is shifted to the lower frequency range (950 cm^{-1}) and for metakaolin, it is shifted to the higher frequency range (1050 cm^{-1}). Bands at 550 and 700 cm^{-1} are also observed, which reflect the deformation and symmetric valence oscillations of alumina-oxygen tetrahedra. They are again shifted to a higher frequency range for metakaolin. The fundamental difference between the spectra of fresh samples and catalysts after the reaction is the bifurcation of the band at 1000 cm^{-1} . The latter can be caused by non-planar oscillations of the terminal vinyl group $\delta\text{-CH}$ in the limonene molecule, which are reflected by the absorption band at 995–985 cm^{-1} .

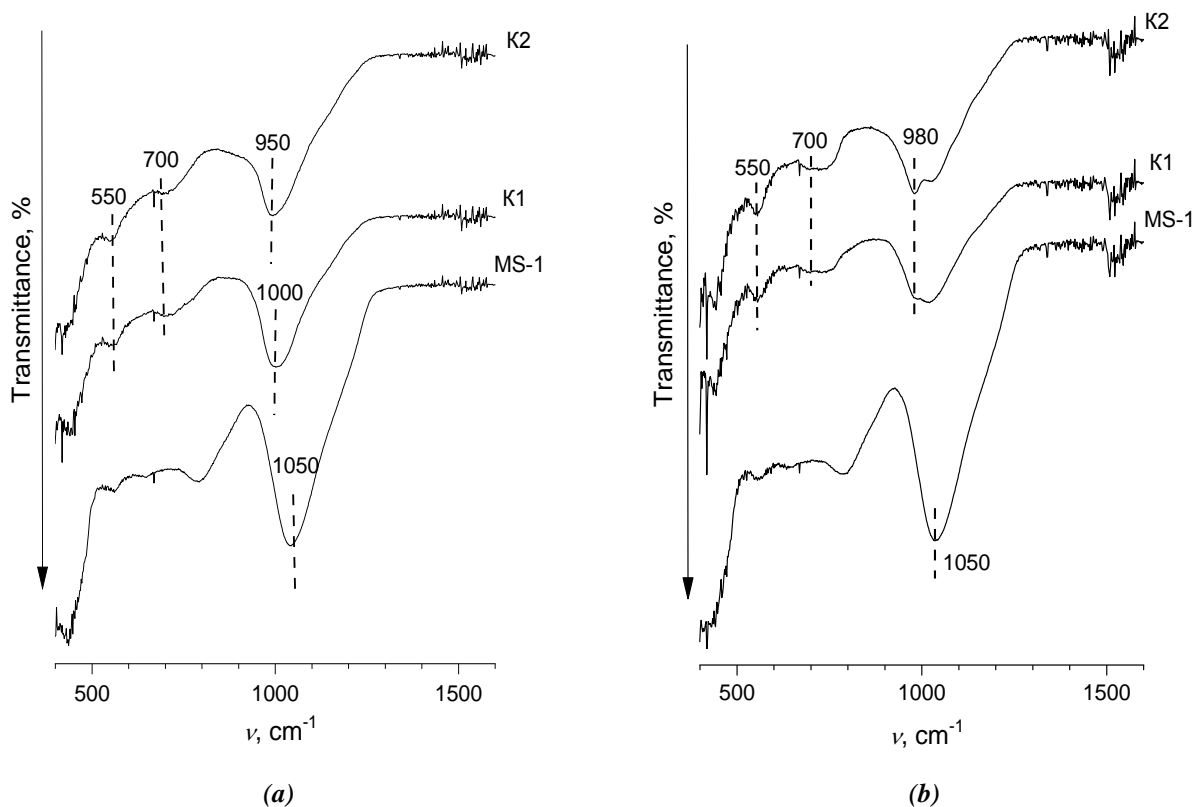


Figure 9. IR spectra of fresh (a) and deactivated (b) in limonene transformation catalysts.

Conclusions

Two faujasite-type zeolite-containing catalysts from Ukrainian kaolin were synthesized. The acid catalysts were prepared by successive ion exchanges of the native zeolite sodium for calcium, lanthanum, and ammonium. The Brønsted and Lewis acidity of the samples was confirmed by pyridine adsorption with IR control.

The XRD and XRF data show that the zeolite phase is represented by X-type zeolite with minor admixtures of aluminosilicate spinel. The SiO₂ to Al₂O₃ ratio for two samples is close to 2. The biporous structure of the samples with varying amounts of micro- and mesopores is confirmed by low-temperature nitrogen adsorption/desorption.

Limonene isomerization on biporous zeolite-containing catalysts synthesized from Ukrainian kaolin was conducted for the first time. The possibility of limonene isomerization on micro-mesoporous zeolite-containing materials is demonstrated, with the increased mesoporosity aiding in the reduction of reaction time.

It was found that the original metakaolin microsphere primarily catalyzes terpene dimerization, whereas terpinolene is the main product of isomerization on polycationic zeolite-containing catalysts. For an 80–90% conversion rate, the maximum yield of isomers is 60–65%. Because limonene has high solubility, it helps to remove intermediate products from the surface of the samples. It was discovered that neither the original microsphere nor the catalysts had a significant accumulation of coke precursors.

Acknowledgments

The publication contains the results of studies conducted with a grant from the National Research Foundation of Ukraine project 2020.01/0042.

References

- Esteban, J.; Yustos, P.; Ladero, M. Catalytic processes from biomass-derived hexoses and pentoses: a recent literature overview. *Catalysts*, 2018, 8(12), pp. 637–678. DOI: <https://doi.org/10.3390/catal8120637>
- Teong, S.P.; Yi, G.; Zhang, Yu. Hydroxymethylfurfural production from bioresources: past, present and future. *Green Chemistry*, 2014, 16(4), pp. 2015–2026. DOI: <https://doi.org/10.1039/C3GC42018C>
- Satira, A.; Espro, C.; Paone, E.; Calabrò, P.S.; Pagliaro, M.; Ciriminna, R.; Mauriello, F. The limonene biorefinery: from extractive technologies to its catalytic upgrading into *p*-cymene. *Catalysts*, 2021, 11(3), pp. 387–403. DOI: <https://doi.org/10.3390/catal11030387>
- Makarouni, D.; Lycourghiotis, S.; Kordouli, E.; Bourikas, K.; Kordulis, C.; Dourtoglou, V. Transformation of limonene into *p*-cymene over acid activated natural mordenite utilizing atmospheric oxygen as a green oxidant: a novel mechanism. *Applied Catalysis B: Environmental*, 2018, 224, pp. 740–750. DOI: <https://doi.org/10.1016/j.apcatb.2017.11.006>
- Patrylak, L.K.; Pertko, O.P.; Yakovenko, A.V.; Voloshyna, Yu.G.; Povazhnyi, V.A.; Kurmach, M.M. Isomerization of linear hexane over acid-modified nanosized nickel-containing natural Ukrainian zeolites. *Applied Nanoscience*, 2022, 12, pp. 411–425. DOI: <https://doi.org/10.1007/s13204-021-01682-1>
- Brei, V.V.; Melezhyk, O.V.; Prudius, S.V.; Levchuk, M.M.; Patryliak, K.I. Superacid WO_x/ZrO₂ catalysts for isomerization of *n*-hexane and for nitration of benzene. *Studies in Surface Science and Catalysis*, 2002, 143, pp. 387–395. DOI: [https://doi.org/10.1016/S0167-2991\(00\)80679-5](https://doi.org/10.1016/S0167-2991(00)80679-5)
- Johnson, Jr.W.E. Process for the isomerization of limonene to terpinolene. USA Patent, 1985, No. US4551570A. <https://patents.google.com/patent/US4551570A/en>
- Aricu, A. The natural product chemistry of terpenoids – a tribute to the remarkable legacy of academician Pavel Vlad. *Chemistry Journal of Moldova*, 2021, 16(1), pp. 8–29. DOI: <http://dx.doi.org/10.19261/cjm.2021.856>
- Ito, K.; Ito, M. The sedative effect of inhaled terpinolene in mice and its structure–activity relationships. *Journal of Natural Medicines*, 2013, 67, pp. 833–837. DOI: <https://doi.org/10.1007/s11418-012-0732-1>
- Deck, P.; Birkert, O. Addition of H₂S to terpenes for producing novel molar mass regulators for radical polymerisations. USA Patent, 2010, No. US20100010267A1. <https://patents.google.com/patent/US20100010267A1/en>
- Okumura, N.; Yoshida, H.; Nishimura, Yu.; Kitagishi, Ya.; Matsuda, S. Terpinolene, a component of herbal sage, downregulates AKT1 expression in K562 cells. *Oncology Letters*, 2012, 3(2), pp. 321–324. DOI: <https://doi.org/10.3892/ol.2011.491>
- Ma, Y.; Marston, G. Formation of organic acids from the gas-phase ozonolysis of terpinolene. *Physical Chemistry Chemical Physics*, 2009, 11(21), pp. 4198–4209. DOI: <https://doi.org/10.1039/b818789d>
- Ikeda, Yo.; Takamatsu, C.; Matsuyama, K. Raw-material for pregellation, method for preparation of pregel, pregel, method for production of molded material, and molded material. European Patent, 1990, No. EP0376662A2. <https://patents.google.com/patent/EP0376662A2/en>
- Retajczyk, M.; Wróblewska, A.; Szymańska, A.; Michalkiewicz, B. Isomerization of limonene over natural zeolite-clinoptilolite. *Clay Minerals*, 2019, 54(2), pp. 121–129. DOI: <https://doi.org/10.1180/clm.2019.18>

15. Martin-Luengo, M.A.; Yates, M.; Rojo, E.S.; Arribas, D.H.; Aguilar, D.; Hitzky, E.R. Sustainable *p*-cymene and hydrogen from limonene. *Applied Catalysis A: General*, 2010, 387(1-2), pp. 141–146. DOI: <https://doi.org/10.1016/j.apcata.2010.08.016>
16. Catrinescu, C.; Fernandes, C.; Castilho, P.; Breen, C. Influence of exchange cations on the catalytic conversion of limonene over Serra de Dentro (SD) and SAz-1 clays: correlations between acidity and catalytic activity/selectivity. *Applied Catalysis A: General*, 2006, 311, pp. 172–184. DOI: <http://dx.doi.org/10.1016/j.apcata.2006.06.023>
17. Retajczyk, M.; Wróblewska, A. Isomerization and dehydroaromatization of *R*(+)-limonene over the Ti-MCM-41 catalyst: effect of temperature, reaction time and catalyst content on product yield. *Catalysts*, 2019, 9(6), pp. 508–519. DOI: <https://doi.org/10.3390/catal9060508>
18. Retajczyk, M.; Wróblewska, A. The isomerization of limonene over the Ti-SBA-15 catalyst – the influence of reaction time, temperature, and catalyst content. *Catalysts*, 2017, 7(9), pp. 273–287. DOI: <https://doi.org/10.3390/catal7090273>
19. Patrylak, L.; Likhnyovskyi, R.; Vypyraylenko, V.; Leboda, R.; Skubiszewska-Zieba, J.; Patrylak K. Adsorption properties of zeolite-containing microspheres and FCC catalysts based on Ukrainian kaolin. *Adsorption Science and Technology*, 2001, 19(7), pp. 525–540. DOI: <https://doi.org/10.1260/0263617011494376>
20. Patrylak, L.K.; Yakovenko, A.V. Alkylation of isobutane with butenes under microcatalytic conditions in pulse mode. *Issues of Chemistry and Chemical Technology*, 2021, 1, pp. 55–61. (in Ukrainian). DOI: <http://dx.doi.org/10.32434/0321-4095-2021-134-1-55-61>
21. Breck, D.W. *Zeolite Molecular Sieves: Structure, Chemistry, and Use*. John Wiley: New York, 1973, 771 p.
22. Rouquerol, F.; Rouquerol, J.; Sing, K. *Adsorption by Powders and Porous Solids: Principles, Methodology and Applications*. Academic Press: San Diego, 1999, 467 p.
23. Barrett, E.P.; Joyner, L.G.; Halenda, P.P. The determination of pore volume and area distributions in porous substances. I. Computations from nitrogen isotherms. *Journal of the American Chemical Society*, 1951, 73(1), pp. 373–380. DOI: <https://doi.org/10.1021/ja01145a126>
24. Ravikovitch, P.I.; Haller, G.L.; Neimark, A.V. Density functional theory model for calculating pore size distributions: pore structure of nanoporous catalysts. *Advances in Colloid and Interface Science*, 1998, 76-77, pp. 203-226. DOI: [https://doi.org/10.1016/S0001-8686\(98\)00047-5](https://doi.org/10.1016/S0001-8686(98)00047-5)
25. Cejka, J.; Van Bekkum, H.; Corma, A.; Schueth, F. Eds. *Introduction to zeolite molecular sieves*. Elsevier: New York, 2007, pp. 787–836. DOI: [https://doi.org/10.1016/S0167-2991\(07\)80810-X](https://doi.org/10.1016/S0167-2991(07)80810-X)
26. Rabo, J.A. *Zeolite chemistry and catalysis*. American Chemical Society: Washington, 1976, 796 p.
27. Lakiss, L.; Vicente, A.; Gilson, J.-P.; Valtchev, V.; Mintova, S.; Vimont, A.; Bedard, R.; Abdo, S.; Bricker, J. Probing the Brønsted acidity of the external surface of faujasite-type zeolites. *ChemPhysChem*, 2020, 21(16), pp. 1873–1881. DOI: <https://doi.org/10.1002/cphc.202000062>
28. Alver, B.E.; Sakizci, M.; Yörükoğullari, E. Investigation of clinoptilolite rich natural zeolites from Turkey: a combined XRF, TG/DTG, DTA and DSC study. *Journal of Thermal Analysis and Calorimetry*, 2010, 100(1), pp. 19–26. DOI: <https://doi.org/10.1007/s10973-009-0118-0>